Available online at www.sciencedirect.com
SCIENCE DIRECT®
Journal of Nuclear Materials 348 (2006) 18–25
journal of nuclear materials
www.elsevier.com/locate/jnucmat

Heat and mass transfer calculations in heavy liquid metal loops under forced convection flow conditions

H. Steiner *, J. Konys

Forschungszentrum Karlsruhe, Institut für Materialforschung III, P.O. Box 3640, 76021 Karlsruhe, Germany

Received 17 December 2004; accepted 30 May 2005

Abstract

The formation of oxide scales on the structural components in a liquid metal system is considered as a viable measure in limiting the dissolution rates in the hot parts. A simple method has been devised to calculate heat and mass transfer in such systems. The method is based on the use of heat and mass transfer coefficients which determine the heat and mass flux from the wall into the fluid. These coefficients depend on characteristic thermo-hydraulic numbers like the Nusselt number and the Sherwood number. This is supplemented by the application of the mass and energy conservation laws to calculate the conditions in the bulk of the fluid. The dissolution and precipitation rates are then coupled to the oxidation kinetics of the structural components in order to calculate the evolution of the oxide scale thickness and the dimensional changes of the channel walls.

1. Introduction

Liquid metal alloys have gained various applications in technical systems during the last decades. Recently, lead–bismuth eutectic (LBE) is foreseen as coolant and target in accelerator driven nuclear systems (ADS). Also, the Pb–17Li alloy is considered as a coolant and breeding medium in future fusion reactors. One major problem in non-isothermal liquid metal systems lies in the corrosion of their structural materials, consisting mainly of martensitic and austenitic stainless steels.

The formation of oxide scales on the structural components is considered as a viable measure in limiting the dissolution rates in the hot parts of the system, as the solubility of the oxides is in general much smaller than that of the metal alloys. Oxide scales might not be stable as for example in the Pb–17Li alloy, but there may also be a problem in LBE loops at low oxygen concentrations. Hence, the prediction of the oxide scale evolution is of great importance. Also precipitation of oxides at cooler parts of the system can have consequences as there may be clogging and plugging of components having small cross-sections. This may also affect maintenance and repair of the system as in an ADS there will be activation of steel components and there will be a transport of activated material.

The locations of dissolution and precipitation are mainly determined by the temperature dependence of the solubility of the oxides or of the metal alloys if no oxide scale is present. This means that we have dissolution in the hot parts of the system and precipitation in the cold parts, irrespective of the nature of the dissolution process, whether it is exothermic or endothermic.

* Corresponding author. Tel.: +49 7247 824113; fax: +49 7247 823956.
E-mail address: helmut.steiner@imf.fzk.de (H. Steiner).

0022-3115/$ - see front matter © 2005 Elsevier B.V. All rights reserved.
doi:10.1016/j.jnucmat.2005.05.013

In a previous paper [1] some information on a recently developed simple model for the calculation of the mass transfer in a liquid metal loop was given. In this paper we are going to discuss this model in more detail and extend it also to heat transfer. We will also establish the link to the oxidation kinetics in order to calculate the evolution of the oxide scales on the structural components.

2. Theory

2.1. Mass transfer

In general, one has forced convection flow conditions in liquid metal loops, either laminar or turbulent flow. If one wants to calculate the transport of ions, atoms, or molecules present in the liquid metal in a certain concentration c_i (with i denoting the solute), one can use the convective diffusion equation (cp. Ref. [2]):

$$\frac{\partial c_i}{\partial t} + (\vec{v}\nabla)c_i = \nabla(D_i \nabla c_i), \tag{1}$$

where is $\vec{v}$ the velocity of the liquid metal and D_i the diffusivity of solute i in the liquid metal. The convective diffusion equation is given in its most general form, assuming that the concentration can depend on the axial position x in the loop and on transversal coordinates and that there can be a transient phase.

Such a procedure has been adopted by Zhang and Li, which have published a series of papers [2–5]. But one can also take a different route for the solution of the problem. Namely, one can take profit of the principles of convective mass transfer, which stipulate that under forced convection flow conditions the mass flux is determined by a dimensionless characteristic flow parameter, the so-called Sherwood number; and we can take profit (if needed) of the analogy between heat and mass transfer. Thus, the mass flux of the solute i from the channel wall into the bulk of the fluid is given by the following equation (cp. Ref. [13]):

$$j_i = K_i^{fl} \cdot (c_i^w - c_i^b), \tag{2}$$

where K_i^{fl} is the mass transfer coefficient for the solute i, c_i^w the concentration of the solute i at the wall and c_i^b is the concentration in the bulk of the fluid.

The direction of the mass flux depends on the ratio of the two concentration values. If c_i^w is higher than c_i^b then the mass flux is directed from the wall into the fluid; if c_i^w is smaller than c_i^b then the mass flux is directed from the fluid to the wall.

In the following we make implicitly use of the fact that the solutions of the thermo hydraulic equations depend on characteristic non-dimensional quantities, which is finally a consequence of Buckingham's Π-theorem [6].

The mass transfer coefficient K_i^{fl} is determined by the Sherwood number Sh in the following way:

$$K_i^{fl} = \frac{D_i}{d_{hyd}} \cdot Sh, \tag{3}$$

where d_{hyd} is the hydraulic diameter.

Bringing the convective diffusion Eq. (1) into a non-dimensional form, one can show that under forced convection flow conditions its solutions depend on the Reynolds number Re and on the Schmidt number Sc. Thus, the Sherwood number Sh, which is the characteristic number for the non-dimensional mass flux must also depend on the Reynolds number and on the Schmidt number. Therefore we have the following functional relationship:

$$Sh = a \cdot Re^{\alpha} \cdot Sc^{\beta}. \tag{4}$$

The parameters a and α, β must be determined experimentally depending on the flow regime.

$$Re = \frac{u_{fl} \cdot d_{hyd}}{\upsilon_{fl}}, \qquad Sc = \frac{\upsilon_{fl}}{D_i}, \tag{5}$$

where υ_{fl} is the kinematic viscosity of the fluid and u_{fl} the flow velocity.

It remains to calculate the solute concentration in the bulk of the fluid c_i^b along the whole loop. This is done with the help of the mass conservation law. In this way we have derived the following differential equation:

$$\frac{\partial c_i^b(t,x)}{\partial t} + u_{fl} \cdot \frac{\partial c_i^b(t,x)}{\partial x} = \frac{U_{ch}}{A_{ch}} \cdot j_i(t,x), \tag{6}$$

where U_{ch} is the circumference of the flow channel, A_{ch} the cross-section of the flow channel and u_{fl} the flow velocity in the coolant channel.

The axial position x in the loop is to be understood as a length of flow path, as the different axial sections of the loop are added in a scalar way irrespective of their orientation in space.

There we have assumed that the bulk concentration does not depend on transverse coordinates, as the concentration c_i^b in the liquid metal is practically uniform, with appreciable concentration differences appearing only in a very thin layer at the wall. This thin layer was neglected in the derivation of Eq. (6).

We have also to fix the boundary conditions. In a closed loop we have the following periodic boundary condition:

$$c_i^b(t,0) = c_i^b(t,L), \tag{7}$$

where L is the total length of the loop. In a pipe flow situation we would have in most cases the following condition at the inlet:

$$c_i^b(t,0) = c_i^0(t), \tag{8}$$

where $x = 0$ is the axial position of the inlet. If there is a magnetic trap at some axial location $x_{m.tr.}$, which is able to remove the solute i quantitatively we would also have

$$c_i^b(t, x_{m.tr.}) = 0. \tag{9}$$

The value which we have to take for c_i^w depends on the nature of the interface. If the solute results from an interface reaction with a rate constant k_s we have a two-step mechanism and the overall mass transfer coefficient K_t is given by [7]

$$K_t = \frac{k_s \cdot K_i^{fl}}{k_s + K_i^{fl}}. \tag{10}$$

When $k_s \gg K_i$ then $K_t \to K_i^{fl}$. We have also assumed that there is no diffusion surface layer, which the solute i must pass. Otherwise, the overall mass transfer coefficient is given by

$$K_t = \frac{K_i^{fl} \cdot D_i^{s.l.}/\delta}{K_i^{fl} + D_i^{s.f.}/\delta}, \tag{11}$$

where $D_i^{s.l.}$ is the diffusion coefficient of the species i in the surface layer and δ the thickness of the surface layer. Using the overall mass transfer coefficient we have the following equation:

$$j_i = K_t \cdot (c_i^s - c_i^b), \tag{12}$$

with c_i^s being the solubility of the species i in the liquid metal.s

2.1.1. Calculation of dissolution and precipitation rates

We have now all the necessary elements for the calculation of the dissolution and the precipitation rates, one of the main aims of this work. We are mainly concerned with stainless steel components and in the foregoing we will derive formulas relevant for this kind of material. If we have an oxide scale consisting of magnetite the dissolution and precipitation rates are given as

$$b_{ox} = -j_{Fe} \cdot \frac{3 \cdot M_{Fe} + 4 \cdot M_O}{3 \cdot M_{Fe}} / \rho_{ox}, \tag{13}$$

where j_{Fe} is the iron flux, M_i the atomic weight of the species i and ρ_{ox} the specific density of the magnetite.

If we have an iron–chromium spinel, the ratio of the atomic weights in Eq. (13) has to be modified accordingly. We have adopted the convention that in case of dissolution the rate b^{ox} is negative and in case of precipitation positive. If there is no oxide scale present, the dissolution and precipitation rates depend a bit on the behavior of all the alloying components. If f_{Fe} measures the mass fraction of all the alloying elements of the cladding dissolved or precipitated which can be attributed to iron, we get:

$$b_{me} = -j_{Fe} \cdot \frac{1}{\rho_{ss} \cdot f_{Fe}}, \tag{14}$$

where ρ_{ss} is specific density of stainless steel. It should be noted that in both cases the calculated iron flux which appears in Eqs. (13) and (14) is very different, as the solubility can differ by order of magnitudes.

2.1.2. Evolution of the oxide scale and variation of the oxygen concentration along the loop

If the concentration of oxygen in the liquid metal is above a certain limiting value, oxide scales are formed on the stainless steel components. We assume that in the absence of dissolution the increase of the oxide scale can be described by some function $r(T, c_O)$ for the oxidation rate, then we can establish the following balance equation for the oxide scale:

$$\frac{d\delta_{ox}(t)}{dt} = r(T, c_O) + b_{ox}, \tag{15}$$

where c_O is the oxygen concentration in the liquid metal.

If oxide scale formation is determined by a parabolic growth law, then we can write

$$\frac{d\delta_{ox}(t)}{dt} = \frac{a_{ox}(T, c_O)}{\delta_{ox}(t)} + b_{ox}, \tag{16}$$

where a_{ox} is the parabolic oxidation rate parameter.

A similar equation has originally been used by Tedmon [8] for high-temperature oxidation with simultaneous volatilization of Cr_2O_3. In the high temperature region we have dissolution, b_{ox} is negative and the oxide scale thickness tends to a limiting value, irrespective of the initial oxide scale thickness:

$$\delta_{ox}^{equi} = \frac{-a_{ox}(T, c_O)}{b_{ox}}. \tag{17}$$

If the initial oxide scale thickness is below the equilibrium value, the oxide scale will grow; if the initial value is above, the oxide scale will decrease. For the equilibrium value of the oxide scale thickness scale formation and dissolution would be in dynamic equilibrium with both processes still continuing. That means the oxide scale would move inwards at a constant rate given by b_{ox}.

In case of precipitation the oxide scale would finally grow linearly:

$$\frac{d\delta_{ox}(t)}{dt} \to b_{ox}. \tag{18}$$

In a time increment Δt the oxide scale thickness will change by $\Delta\delta_{ox}$ and the wall inner radius will change by:

$$\Delta r_i^{ch} = -\left(\frac{r(T, c_O)}{\Phi} + b_{ox}\right) \cdot \Delta t, \tag{19}$$

where Φ is the Pilling–Bedworth ratio. The sign convention is that in case of dissolution b_{ox} is negative and in case of precipitation it is positive. If no oxide scale is present on the inner clad wall, we have:

$$\Delta r_i^{ch} = -b_{me} \cdot \Delta t. \tag{20}$$

Eqs. (15) and (16) determine also the oxygen flux j_O from the wall into the liquid metal:

$$j_O = -(r(c_O, T) + b_{ox}) \cdot \frac{4 \cdot M_O}{3 \cdot M_{Fe} + 4 \cdot M_O} \cdot \rho_{ox}. \quad (21)$$

We can now calculate the change of the oxygen concentration along the loop in the same way as has been done for the iron concentration:

$$\frac{\partial c_O^b(t,x)}{\partial t} + u^{fl} \cdot \frac{\partial c_O^b(t,x)}{\partial x} = \frac{U_{ch}}{A_{ch}} \cdot j_O(t,x), \quad (22)$$

where c_O^b is the oxygen concentration in the bulk of the fluid. If there is oxygen control at some axial location of the loop, the respective oxygen concentration figures as a boundary value at this axial location.

2.2. Heat transfer

If the temperature distribution in a liquid metal system is axially non-homogeneous there will also occur heat transfer beside that of solute elements. Liquid metal systems had been constructed in the past especially for this purpose [9], but in loops like CORRIDA and PICOLO [10,11] this aspect is of minor importance. The modeling of heat transfer follows the same path as that for mass transfer. The heat flux q from the wall into the fluid can be given by

$$q = \frac{Nu \cdot \lambda_{fl}}{d_{hyd}} \cdot (T_w - T_{fl}), \quad (23)$$

where λ_{fl} is the heat conductivity of the fluid.

For liquid metals the Nusselt number Nu is in general represented as a function of the Peclet number Pe, for example by the following correlation recommended by the Liquid-Metals Handbook [12]:

$$Nu = 7.0 + 0.025 \cdot Pe^{0.8} \cdot Pe = Re \cdot Pr, \quad (24)$$

where Pr is the Prandtl number. The change of the liquid metal enthalpy is calculated with the help of the energy conservation law:

$$\frac{\partial(\rho_{fl} \cdot c_p^{fl} \cdot T_{fl})}{\partial t} + u_{fl} \cdot \frac{\partial(\rho_{fl} \cdot c_p^{fl} \cdot T_{fl})}{\partial x} = \frac{U_{ch}}{A_{ch}} \cdot q(t,x), \quad (25)$$

where ρ_{fl} is the liquid metal density and c_p^{fl} the liquid metal heat capacity.

3. Results of calculations and discussion

The newly developed model has been incorporated in the computer code MATLIM, where the relevant differential equations are solved with the help of finite difference techniques by dividing the whole loop into a certain number of axial meshes. In the actual version of the code a value of 1000 axial meshes is used. But this value can easily be increased if there is a need. In this way multi-modular loops can easily be treated, as specific values for the relevant parameters can be assigned for each axial mesh. The calculations were done for the CORRIDA [10] and PICOLO [11] loops. The main characteristics of these loops are described elsewhere and shall therefore not be mentioned in this paper.

There are mainly three different types of physical properties and parameters, which determine material behavior in a liquid metal system. The first group concerns the thermo-hydraulic data of the system like the flow velocity and the hydraulic diameter but also the temperature distribution along the system. The second group concerns material data like viscosity of the liquid metal, diffusivity and solubility of the solutes. The third group encompasses properties of the wall materials itself like oxidation rates. The dependence on the thermo-hydraulic parameters is evident from Eqs. (3) and (4) and will be discussed in the following for turbulent and laminar flow conditions.

There are a number of correlations for the mass transfer coefficient obtained under fully developed turbulent pipe flow. Our main assumption is that they can also be applied for liquid metal loops. Three of these correlations were investigated and discussed in Ref. [13]. These are the correlation of Berger and Hau [14], that of Silverman [15], and that of Harriott and Hamilton [16]. The range of validity for the Berger and Hau correlation is for example given in Ref. [13] as follows:

$$8 \cdot 10^3 \leqslant Re \leqslant 2 \cdot 10^5, 1000 \leqslant Sc \leqslant 6000. \quad (26)$$

All these three correlations give similar values for the mass transfer coefficient. It is therefore sufficient for us to use only one of them, namely that of Silverman [15]:

$$K_{Silv} = 0.0177 \cdot u_{fl}^{0.875} \cdot D_{Fe}^{0.704} / (d_{hyd}^{0.125} \cdot \upsilon_{fl}^{0.567}). \quad (27)$$

In case of laminar flow we can make use of the analogy between heat and mass transfer. There is a lot of information on the heat transfer in pipe flow (laminar and turbulent, inlet flow or fully developed flow) in Ref. [17], which can be applied to mass transfer by replacing the Nusselt number by the Sherwood number and the Prandtl number by the Schmidt number. The model incorporated in the code MATLIM is flexible enough, as in each axial mesh of the loop we can specify the value of the mass transfer coefficient. We are not going to discuss this in all details but give here only the Sherwood number for small values of the parameter $Re \cdot Sc \cdot d_{hyd}/x$ (x = axial distance from the inlet) [17]:

In case of a full circular cross-section:

$$Sh_{la} = 3.66. \quad (28a)$$

In case of an annular cross-section [17]:

$$Sh_{la} = 3.66 + (4 - 0.102/(d_i/d_o + 0.02))(d_i/d_o)^{0.04}, \quad (28b)$$

where d_i, d_o are inner, outer diameter of the flow channel.

There we have made use of the analogy between heat and mass transfer, that means replaced the Nusselt number by the Sherwood number.

We have applied the Nusselt number correlation given in [17] for fixed values of the wall temperature and not that for fixed values of the heat flux, as these values are to be transferred for a situation with fixed values for the concentration of the solutes at the wall. It should be noted that in case of fully developed laminar flow the mass transfer coefficient does not depend on the flow velocity and increases linearly with the iron diffusivity.

The flow in pipes is laminar up to a Reynolds number of 2300 and it becomes fully turbulent at a Reynolds number of 10000. In between we have a transition regime. In order to describe this transition regime we follow the procedure proposed in [17], which is based on a linear interpolation between the Nusselt numbers in the laminar and in the turbulent regime. Defining the parameter γ as

$$\gamma = \frac{Re - 2300}{10^4 - 2300} \tag{29}$$

we obtain the Sherwood number in the transition region as follows:

$$Sh_{tr} = (1-\gamma)\cdot Sh_{la}(2300) + \gamma \cdot Sh_{turb}(10^4). \tag{30}$$

Sh_{turb} is the Sherwood number in the fully turbulent region.

Solubility data for liquid lead–bismuth eutectic (LBE) are given in Ref. [2]. In case of the pure metal without an oxide scale the solubility of iron in LBE is accordingly:

$$c^s_{Fe}(T) = 10^{6.01-4380/T} \quad \text{(in wppm)}. \tag{31}$$

If there is an Fe_3O_4 oxide scale present, the solubility is according to Ref. [2]:

$$c^s_{Fe}(T, c_O) = c_O^{-1.33}\cdot 10^{11.35-12844/T} \quad \text{(in wppm)}, \tag{32}$$

where T is the temperature in K and c_O the oxygen concentration in LBE.

In Ref. [2] are also given solubility data for Ni, Cr and O. It should be noted that the data for oxygen are different from those given in [18] and also those in [19]. To the knowledge of these authors none of these solubility correlations have been validated experimentally.

As long as there is an oxide scale present on the metallic surface, Eq. (32) is to be applied irrespective of the fact that, below a limiting value of the oxygen concentration, correlation (31) provides then lower values.

For Pb–17Li, the following correlation for the iron solubility was given in Refs. [13,20,21]:

$$c^s_{Fe}(T) = 10^{2.524-655.07/T} \quad \text{(in wppm)}. \tag{33}$$

The solubility data in Ref. [22] on the other hand would give values lower by about a factor of 1000.

The diffusivity of single-atom solutes in liquid metals can be calculated with the help of the Sutherland–Einstein equation [2]:

$$D_i(T) = \frac{k\cdot T}{4\cdot\pi\cdot\eta_{fl}(T)\cdot r_i}, \tag{34}$$

where η_{fl} is the dynamic viscosity of the fluid and r_i the atomic radius of the solute.

With an atomic radius of 1.13×10^{-40} m for iron [13] and a dynamic viscosity of 1.23×10^{-3} Pa s for LBE at 550 °C, one obtains for the diffusivity of iron in LBE the following value:

$$D_{Fe}(550\,^\circ\text{C}) = 6.5\times10^{-9}\ \text{m}^2/\text{s}. \tag{35}$$

A similar value has been obtained with the Sutherland-Einstein equation for the iron diffusivity in Pb–17Li at 500 °C [13]. This theoretical value was compared to values of the diffusivity obtained from experiments with a rotating cylinder, which are smaller by a factor of about 10^{-5}.

But one should be cautious in applying Eq. (34) for solutes in liquid metals, as they exist in form of solvated metal clusters. Thus, one should use an effective cluster radius in Eq. (34), which can be much larger than the 'real' atomic radius. But it seems doubtful whether a factor of 10^{-5} can be explained in this way. The same problem was also discussed in [25]. There, an iron solubility which is lower by a factor of 1000 was favored. This would allow the use of a much higher iron diffusivity.

It seems that also in LBE the iron diffusivity obtained from the Sutherland-Einstein equation gives values for the dissolution rate, which are too high by some orders of magnitude (see below). For the time being we do not know whether this is only due to the iron diffusivity or may be also to the iron solubility.

In general, diffusion is a slow process compared to chemical reactions. Therefore we assume that the rate constant of the interface reaction,

$$Fe_3O_4 + 4Pb \rightarrow 3Fe + 4PbO \tag{36}$$

is much higher than the mass transfer coefficient in the liquid metal. Thus, we have:

$$c^w_{Fe} = c^s_{Fe}, \qquad K_t = K^{fl}_{Fe} \tag{37}$$

with c^w_{Fe} the concentration of Fe at the wall and c^s_{Fe} the solubility of Fe in the liquid metal.

This view is generally accepted in the literature (see for example Refs. [2,13]). In case of metallic surfaces, as in the PICOLO loop, we also assume that there is no diffusion layer at the surface of the wall. This condition can be removed, if in the future we can get experimental evidence for such surface layers. According to

Ref. [21] porous ferritic layers are observed on the surface of austenitic steels which are characterized by a depletion of nickel, manganese and chromium. On the other hand, ferritic steels, show no such surface layer [21]. The presence of porous surface layers could eventually be not observed by metallography, as they may be very friable. They would in any case necessitate the use of a much lower iron diffusivity in the liquid metal than in reality, if they are not included in the model.

The main features of the two loops for which calculations have been done are listed in Table 1.

In Fig. 1 we have plotted the axial temperature distributions along the loop. In Figs. 2–6 results of calculations for the CORRIDA loop are seen.

Fig. 2 shows the axial distribution of the iron flux from the wall into the liquid metal and the iron concentration in the bulk of the fluid for a value of the iron diffusivity of 2×10^{-10} m^2/s. The latter parameter influences also the iron flux, as for constant wall temperature the iron flux decreases with increasing iron concentration in the bulk.

Table 1
Main characteristics of the CORRIDA and PICOLO loops

Loop specification	CORRIDA	PICOLO
Coolant	LBE	Pb–17Li
Temp. cold leg (°C)	400	350
Temp. hot leg (°C)	550	480–550
Hydr. diameter (mm)	16	8
Total length (m)	35.8	10.6
Flow velocity (cm/s)	200	30
Oxygen content (wppm)	0.01	$<10^{-5}$

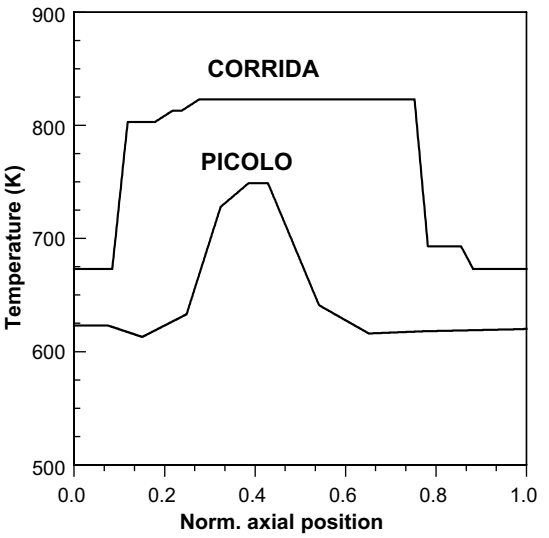

Fig. 1. Axial temperature distributions in CORRIDA and PICOLO loops.

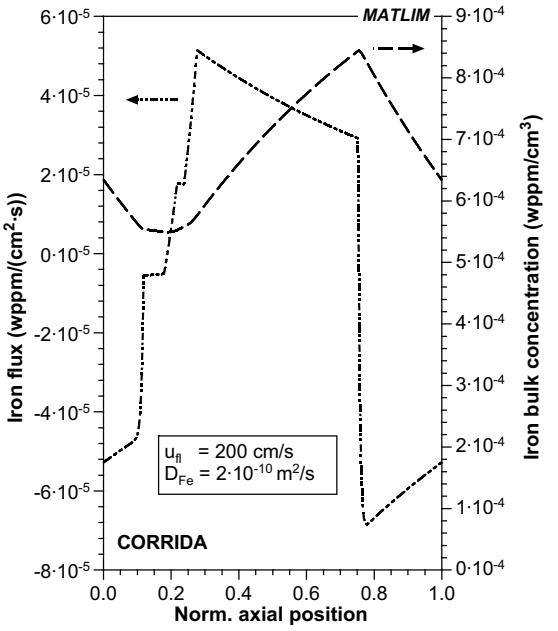

Fig. 2. Axial distributions of the iron flux and iron concentration in the bulk of the fluid.

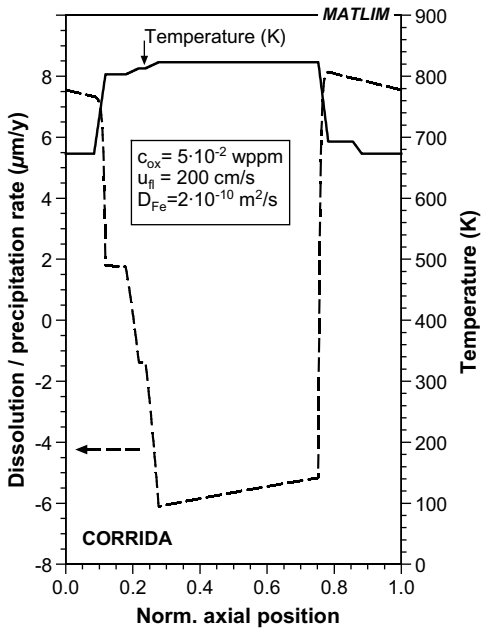

Fig. 3. Axial distributions of the dissolution/precipitation rates (CORRIDA).

In Fig. 3, the axial distribution of the dissolution/precipitation rate in μm/y is plotted. For the time being we have no experimental values of the dissolution rate, but we expect it to range between 1 and 10 μm/y. It is known

that the dissolution rates can be rather high for metallic surfaces.. A value of 0.37 mm/y for the steel DIN 1.4914 in flowing Pb–17Li is given in Ref. [23]. For oxide scales the dissolution rates should be lower by at least one or two orders of magnitude. For the selected value of the iron diffusivity we have obtained a maximum dissolution rate of about 6 μm/y with a value of the oxygen concentration in the liquid metal of 0.05 wppm.

Fig. 4 shows a similar study on the maximum dissolution rate in the CORRIDA loop with a variation of the iron diffusivity and the oxygen concentration in the liquid metal. The dissolution rate becomes rather high for oxygen concentrations below about 0.01 wppm, and in this range the sensitivity on the iron diffusivity is rather obvious. For the time being we have no experimental data for the dissolution rate of magnetite. But we expect that they are relatively small (<10 μm/y) and this would then mean that the iron diffusivity as obtained from the Sutherland-Einstein equation is probably higher by about two orders of magnitude.

Values of the equilibrium oxide scale thickness at 550 °C for the martensitic steel DIN 1.4910 in dependence on the dissolution rate are seen in Fig. 5 and in Fig. 6 the evolution of the oxide scale thickness for a dissolution rate of 10 μm/y. About 20 000 h of operational time are needed to reach more than 95% of the equilibrium value of the oxide scale thickness. We have assumed that the unperturbed oxidation is parabolic.

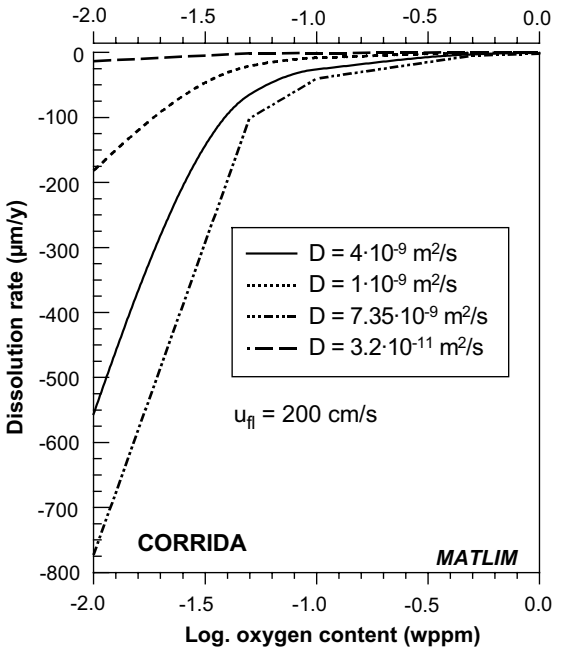

Fig. 4. Maximum dissolution rates versus the oxygen content in the liquid metal.

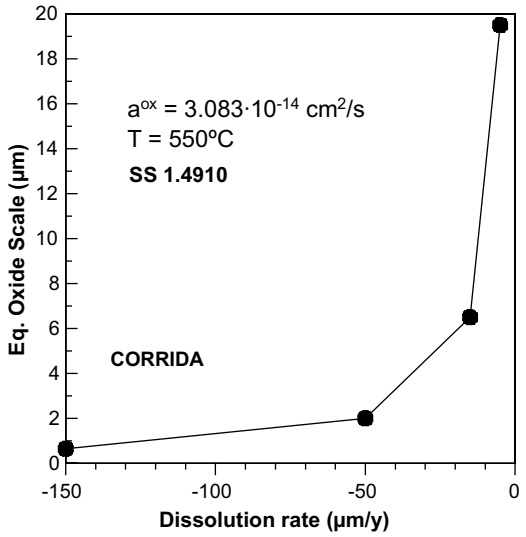

Fig. 5. Equilibrium oxide scale versus the dissolution rate.

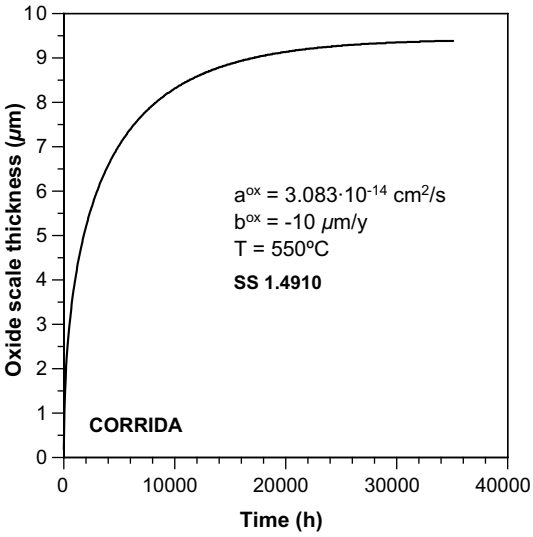

Fig. 6. Evolution of the oxide scale thickness.

The dissolution/precipitation rates in the PICOLO loop for iron diffusivity values of 1×10^{-13} and 2×10^{-13} m^2/s are seen in Fig. 7.

The maximum dissolution rate for these diffusivity values is about 70 and 120 μm/y, respectively, whereas a value of about 100 μm/y has been observed in long term corrosion tests in the PICOLO loop [24]. Thus, the finding of Ref. [13] that the effective iron diffusivity in Pb–17Li is by about five orders of magnitude smaller than given by the Sutherland-Einstein equation is qualitatively confirmed. The calculations were based on the

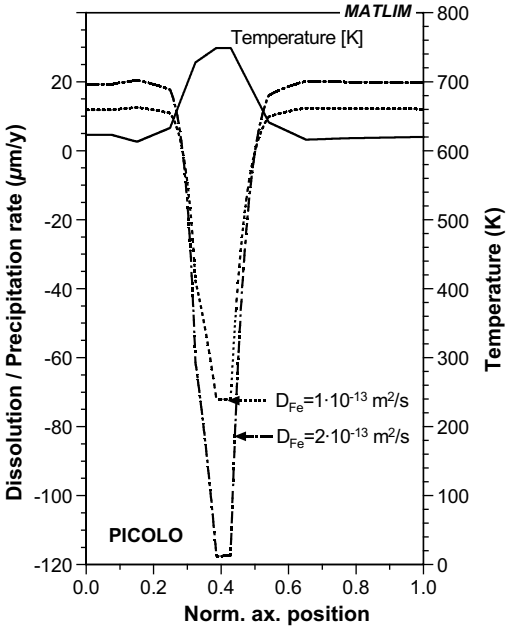

Fig. 7. Axial distributions of the dissolution/precipitation rates (PICOLO).

use of the iron solubilities given in [20,21]. With values of the iron solubility as recommended in [22,23] one would have to take much higher values for the iron diffusivity in order to obtain reasonable values for the dissolution rates. One should also note that the maximum dissolution rate does not only depend on the temperature in the hot leg but also on the temperature distribution along the whole loop. A comparative study using a modified temperature distribution from the CORRIDA loop with a temperature of 480 °C in the hot leg yielded maximum dissolution rates, which were lower by about 40%.

4. Conclusion

A kinetic model for the calculation of heat and mass transfer in liquid metal systems under forced convection flow conditions has been developed. It is based on the use of the relevant characteristic thermo-hydraulic numbers, which determine mass and heat flux from the wall into the fluid. This is supplemented by the application of the mass and energy conservation laws to calculate the conditions in the bulk of the fluid. The oxidation kinetics of the structural components is then combined with the dissolution/precipitation rates for the determination of their geometrical changes if the oxygen content in the liquid metal is high enough.

For metallic surfaces the dissolution rates can be considerable. In this case a lot of experimental data are available. If oxide scales are present the dissolution rates should be very much smaller. No experimental data for dissolution rates in LBE loops are for the time being available. Besides the thermo-hydraulic parameters like flow velocity and hydraulic diameter, iron diffusivity and solubility are of greatest importance. It seems that the effective iron diffusivity is much smaller than given by the Sutherland-Einstein equation.

References

[1] T. Malkow, H. Steiner, H. Muscher, J. Konys, J. Nucl. Mater. 335 (2004) 199.
[2] X. He, N. Li, M. Mineev, J. Nucl. Mater. 297 (2001) 214.
[3] J. Zhang, N. Li, J. Nucl. Mater. 321 (2003) 184.
[4] J. Zhang, N. Li, Corrosion 60 (2004) 331.
[5] J. Zhang, N. Li, J. Nucl. Mater. 326 (2004) 201.
[6] E. Buckingham, Phys. Rev. 4 (1914) 345.
[7] S.Z. Beer, Liquid Metals, Marcel Dekker, N.Y., 1972, 38.
[8] C.S. Tedmon, J. Electrochem. Soc. 113 (1966) 766.
[9] J. Sannier, G. Santarini, J. Nucl. Mater. 107 (1982) 196.
[10] H. Glasbrenner, J. Konys, Z. Voß, J. Nucl. Mater. 281 (2000) 225.
[11] J.U. Knebel, X. Cheng, C.-H. Lefhalm, G. Müller, G. Schumacher, J. Konys, H. Glasbrenner, Nucl. Eng. Des. 202 (2000) 279.
[12] R.N. Lyon, Chem. Eng. Progr. Symp. Ser. 47 (2) (1951) 75.
[13] F. Balbaud-Celerier, F. Barbier, J. Nucl. Mater. 289 (2001) 227.
[14] F.P. Berger, K. Hau, Int. J. Heat Mass Tran 20 (1977) 1185.
[15] D.C. Silverman, Corrosion 55 (1999) 1115.
[16] P. Harriott, R.M. Hamilton, Chem. Eng. Sci. 20 (1965) 1073.
[17] Verein Deutscher Ingenieure, VDI-Wärmeatlas, Berechnungsblätter für den Wärmeübergang, 8. Auflage 1997, Springer-Verlag Berlin Heidelberg, Ga1-Gb5.
[18] A. Heinzel, report FZKA 6823, 2003.
[19] B.F. Gromov, Yu.I. Orlov, P.N. Martynov, V.A. Gulevski, Proc. Conf. Heavy Liquid Metal Coolant in Nucl. Technologies, Obninsk (1998).
[20] M.G. Barker, V. Coen, H. Kolbe, J.A. Lees, L. Orecchia, T. Sample, J. Nucl. Mater. 155–157 (1988) 732.
[21] M.G. Barker, T. Sample, Fus. Eng. Des. 14 (1991) 219.
[22] H.U. Borgstedt, H.D. Röhrig, J. Nucl. Mater. 179–181 (1991) 596.
[23] H.U. Borgstedt, G. Drechsler, G. Frees, Z. Peric, J. Nucl. Mater. 155–157 (1988) 728.
[24] J. Konys, W. Krauss, Z. Voss, O. Wedemeyer, J. Nucl. Mater. 329–333 (2004) 1379.
[25] H.U. Borgstedt, C. Guminski, J. Nucl. Mater. 303 (2002) 240.